JOURNAL OF GEOPHYSICAL RESEARCH, VOL. 104, NO. B11, PAGES 25,221–25,232, NOVEMBER 10, 1999

Coseismic deformation associated with the November 1995, M_W=7.1 Nuweiba earthquake, Gulf of Elat (Aqaba), detected by synthetic aperture radar interferometry

Gidon Baer,[1] David Sandwell, Simon Williams, and Yehuda Bock

Cecil H. and Ida M. Green Institute of Geophysics and Planetary Physics
Scripps Institution of Oceanography, La Jolla, California.

Gadi Shamir

Geophysical Institute of Israel, Holon, Israel

Abstract. The November 22, 1995, M_W=7.1 Nuweiba earthquake occurred along one of the left-stepping segments of the Dead Sea Transform in the Gulf of Elat (Aqaba). Although it was the largest earthquake along this fault in the last few centuries, little is yet known about the geometry of the rupture, the slip distribution along it, and the nature of postseismic deformation following the main shock. In this study we examine the surface deformation pattern during the coseismic phase of the earthquake in an attempt to better elucidate the earthquake rupture process. As the entire rupture zone was beneath the waters of the Gulf, and there is very little Global Positioning System (GPS) data available in the region for the period spanning the earthquake, interferometric synthetic aperture radar (INSAR) provides the only source of information of surface deformation associated with this earthquake. We chose four synthetic aperture radar (SAR) scenes of about 90x90 km each spanning the rupture area, imaged by the ERS-1 and ERS-2 satellites. The coseismic interferograms show contours of equal satellite-to-ground range changes that correspond to surface displacements due to the earthquake rupture. Interferograms that span the earthquake by 1 week show similar fringe patterns as those that span the earthquake by 6 months, suggesting that postseismic deformation is minor or confined to the first week after the earthquake. A high displacement gradient is seen on the western side of the Gulf, 20-40 km south of Elat and Aqaba, where the total satellite-to-ground range changes are at least 15 cm. The displacement gradient is relatively uniform on the eastern side of the Gulf, and the range changes are less than 10 cm. To interpret these results, we compare them to synthetic interferograms generated by elastic dislocation models with a variety of fault parameters. Although selecting the best fit fault parameters is nonunique, we are able to generate a group of simplified model interferograms that provide a reasonable fit to the coseismic interferogram and serve to constrain the location of the fault. The present analysis shows that if the rupture reached the Gulf-bottom surface, the mean sinistral slip along the fault is constrained to about 1.4 m. If surface rupture did not occur, the average sinistral slip is constrained to the range of 1.4-3 m for a fault patch buried 0-4 km below the Gulf-bottom surface, respectively, with a minor normal component.

1. Introduction

Determination of coseismic displacement by geodetic measurements has become an important tool in the last few decades for elucidating earthquake rupture processes. Coseismic displacements have been determined by Global Positioning System (GPS) measurements for at least 15 recent earthquakes [e.g., *Segall and Davis*, 1997, and references therein]. The 1992 M_W=7.3 Landers, California, earthquake was the first large earthquake to be analyzed by both GPS [e.g., *Bock et al.*, 1993] and interferometric synthetic aperture radar (INSAR) [e.g., *Massonnet et al.*, 1993]. Since then, coseismic movements have been determined by INSAR for other earthquakes [*Massonnet et al.*, 1996; *Murakami et al.*, 1996; *Ozawa et al.*, 1997; *Tobita et al.*, 1998]. While the GPS and INSAR methods complement each other very well [*Bock and Williams*, 1997], the INSAR method is particularly advantageous for analyzing earthquakes where GPS measurements are scarce or unavailable and radar ground surface decorrelation is minimal owing to arid conditions. An example of that situation is the November 22, 1995, M_W=7.1 Nuweiba earthquake along the southern section of the Dead Sea Transform (DST).

The Nuweiba earthquake was the largest earthquake to occur along the DST (Figure 1) during the last few centuries [*Ambraseys and Melville*, 1989]. It was strongly felt in Egypt, Israel, Jordan, and Saudi Arabia and caused minor damage to

[1]On Sabbatical from Geological Survey of Israel, Jerusalem.

Paper number 1999JB900216
0148-0227/99/1999JB900216$09.00

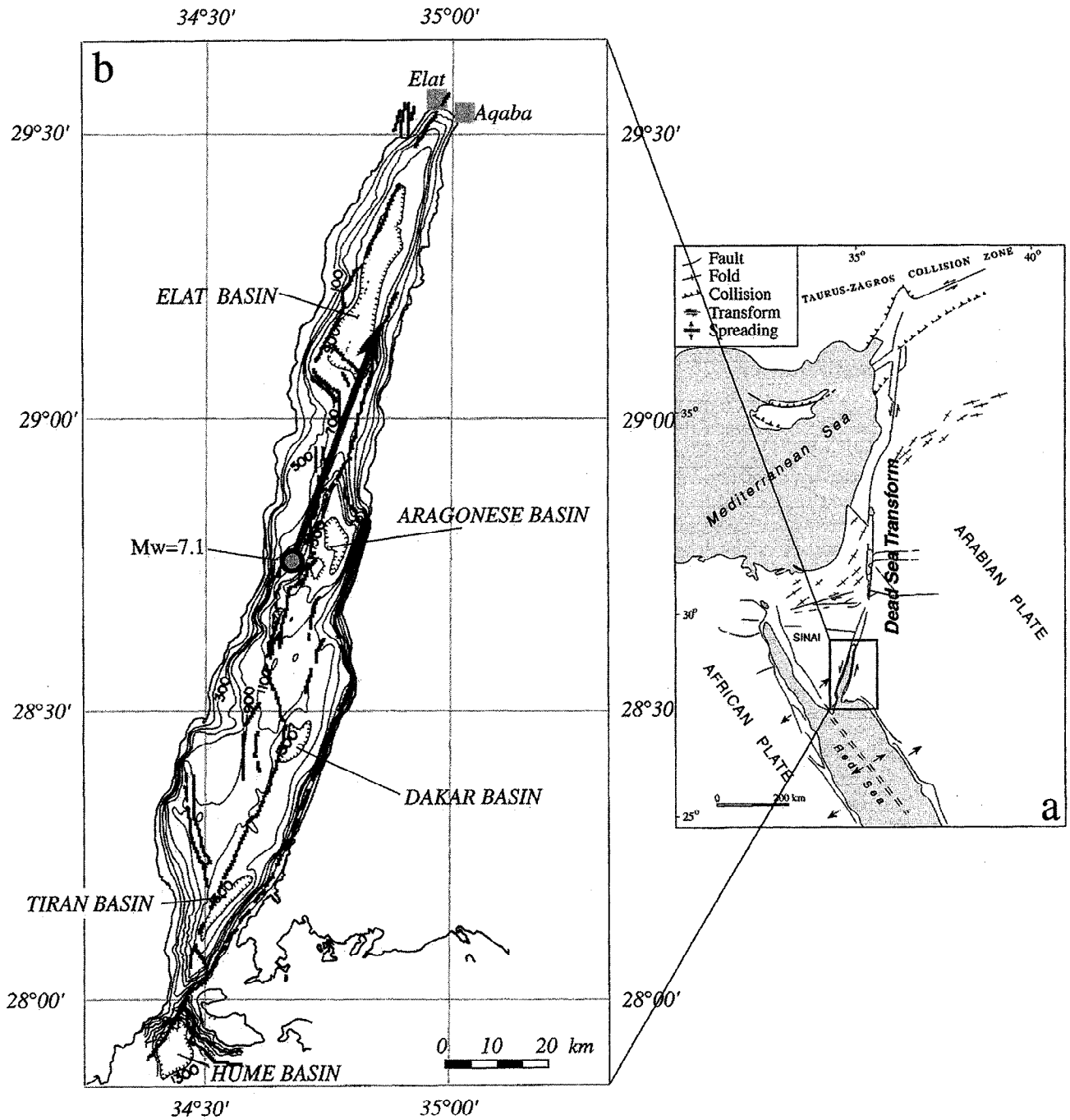

Figure 1. (a) General tectonic setting for the Nuweiba earthquake [modified after *Joffe and Garfunkel*, 1987]. (b) Bathymetry and fault structure of the Gulf of Elat (Aqaba) [modified after *Hall and Ben-Avraham*, 1978; *Ben-Avraham et al.*, 1979; *Ben-Avraham*, 1985; *Ben-Avraham and Tibor*, 1993]. Also shown are the epicenter and the general rupture trace of the Nuweiba earthquake [*Shamir*, 1996].

population centers in the Sinai Peninsula (Egypt), Elat (Israel), and Aqaba (Jordan) [*Wust*, 1997]. Since the entire rupture zone was underwater, there were no direct observations related to rupture geometry and slip distribution. Estimation of these parameters from seismological observations was given by *Shamir* [1996]. The main objective of this study is to utilize the coseismic surface deformation patterns observed geodetically in order to further constrain estimates of rupture geometry and total slip distribution. GPS campaigns in Israel, Jordan, and Egypt included a few measurements before and after the earthquake in the region surrounding the earthquake rupture. Time series of the baseline Bar Giora - Elat (which are located in Israel, 350 and 100 km north of the epicenter, respectively) show southward displacement of Elat by 18.1 ± 1.2 mm with respect to Bar Giora due to the earthquake [*Bechor*, 1998]. Coseismic displacement of 166 mm with azimuth 246° was also identified in Dahab (Egypt), about 26 km southwest of the

epicenter [*Kimata et al.*, 1997]. The displacement of Aqaba (Jordan), about 5 km east of Elat, is still poorly resolved [Ostrovsky, 1997]. As this GPS data is limited in spatial coverage and resolution, additional geodetic data, such as INSAR measurements, are required to resolve the rupture parameters and improve our understanding of this earthquake.

SAR data are available from the ERS-1 satellite, which imaged the area between April 1992 and October 1997, and from the ERS-2 satellite, which has been imaging the area since July 1995. During the overlapping period the two satellites performed tandem missions (at 1 day intervals). For this study we select four SAR scenes of about 90x90 km each in the region surrounding the earthquake that were imaged 8 months and 3 months before the earthquake and 1 week, 6 months, and 26 months after the earthquake. We first generate maps of interferometric fringes (interferograms) of the four scenes by differencing the radar phase measurements acquired before and after the earthquake. The fringes correspond to contours of equal change in satellite-to-ground range and thus define the satellite-to-ground component of the coseismic deformation. Then we compare the observed coseismic interferogram with a synthetic interferogram that is derived from an elastic dislocation model, with fault parameters obtained from the available seismological data. Finally, we vary the fault parameters to minimize the differences between the synthetic and the observed interferograms in order to constrain fault geometry and total fault slip.

2. Nuweiba Earthquake

2.1. Tectonic Setting

The Gulf of Elat (Aqaba) is about 180 km long, 10-25 km wide, and reaches a maximum depth of 1850 m in its central basin [*Ben-Avraham et al.*, 1979]. It forms the inner, active core of a 60-80 km wide deformation zone that constitutes the southern segment of the Dead Sea Transform [*Eyal et al.*, 1981]. This fault connects the Red Sea spreading center in the south, with the Taurus-Zagros collision zone in the north. The total amount of sinistral strike slip along it is about 105 km [e.g., *Quennel*, 1959; *Freund*, 1970], of which at least 30 km has taken place since the Miocene [*Joffe and Garfunkel*, 1987]. West of the Gulf, in eastern Sinai, the deformation zone is manifested by a system of Neogene strike-slip faults, subparallel to the Gulf, which have a total sinistral offset of 24 km [*Bartov et al.*, 1980; *Eyal et al.*, 1981]. The Gulf is bordered by coastal normal faults, which probably ceased to be active prior to the formation of the present Gulf structures [*Eyal*, 1973; *Eyal et al.*, 1981]. Most of the Gulf is occupied by three elongated, fault-bounded basins striking NNE (Figure 1b). The major faults of the Gulf are arranged en echelon, with transverse, probably normal faults at the basin ends. The basins are thus expressions of extension at the step zones [*Ben-Avraham et al.*, 1979], in accordance with the geological sinistral offset along the transform.

2.2. Seismicity

Seismicity in the Gulf in the period of 12 years prior to the Nuweiba earthquake was clustered in space and time and related to the release of energy localized at the Elat/Aragonese and Aragonese/Arnona fault step zones (Figure 1) [*Shamir*, 1996]. The Nuweiba earthquake was preceded by earthquake swarms near both ends of the ruptured segment in 1983, 1990-1991, and 1993 [*El Isa et al.*, 1984; *Alamri*, 1991; *Shamir and Shapira*, 1994]. It was followed by intense aftershock activity, including nearly 200 events of $M_L \geq 4$ in the year following the main shock [*Hofstetter et al.*, 1998]. The epicenter of the Nuweiba earthquake was at 28.76°N, 34.66°E, with an estimated nucleation depth of 12.5 km. Waveform inversions of teleseismic observations [*Kikuchi*, 1995; *Pinar and Turkelli*, 1997] suggest that the rupture consisted of two subevents of sinistral NNE striking faults. On the basis of the *Kikuchi* [1995] waveform inversion, *Shamir* [1996] estimated a total rupture length of 45 km and a total mean dislocation of 3.2 m. *Pinar and Turkelli* [1997] estimated dislocations of only 0.4 and 0.9 m for the first and second subevents, respectively.

3. SAR Processing

SAR processing in this study included the following steps:

1. We first selected four frames (about 90x90 km each) around the earthquake rupture trace, for which ERS data were collected before and after the earthquake (Figure 2). To choose interferometric pairs for topographic correction we searched the listings of ERS data collected in these frames for pairs that do not span the earthquake and have the longest perpendicular baselines (see Figure 3) that still make phase unwrapping (resolving the integer number of 2π cycles) possible (usually up to 200 m). Tandem pairs are preferred because they are taken only 1 day apart and therefore include

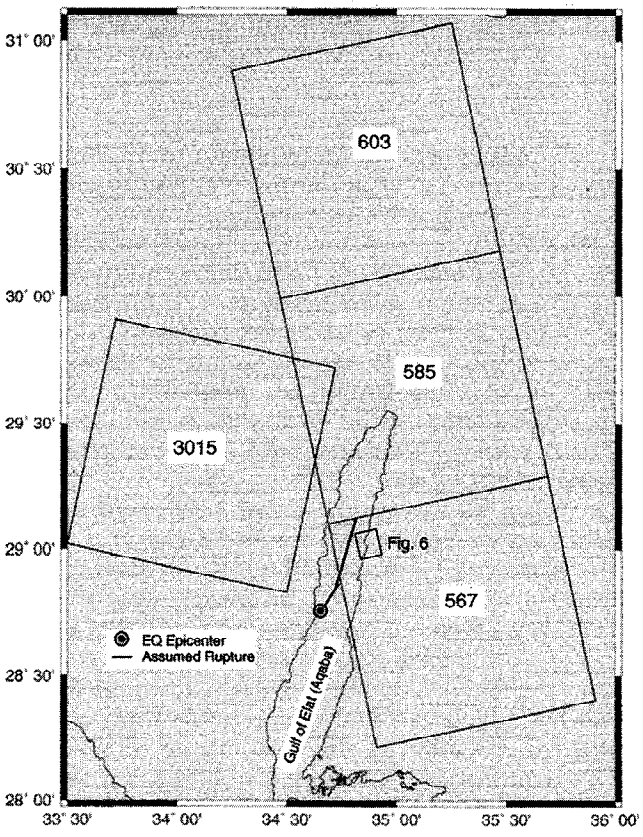

Figure 2. The four synthetic aperture radar (SAR) frames in the vicinity of the Nuweiba earthquake selected for interferometric analysis.

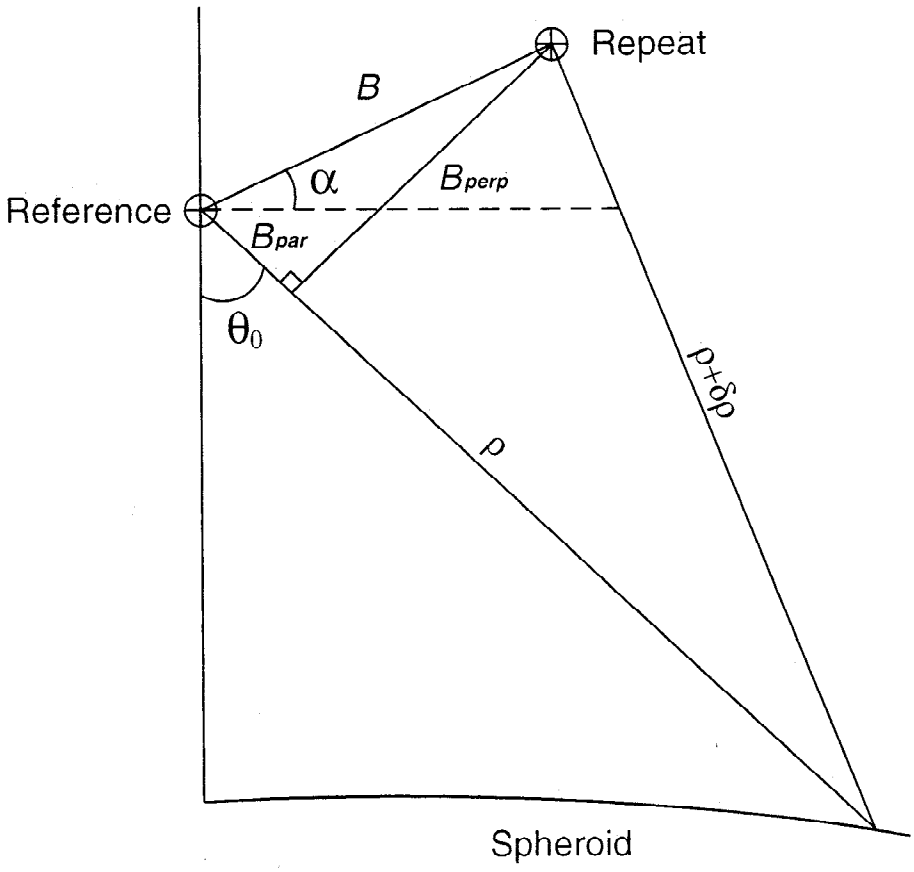

Figure 3. Interferometric SAR (INSAR) geometry for a spheroidal Earth with no topography or deformation. B is the baseline length; B_{par} and B_{perp} are the components of baseline parallel and perpendicular to the line of site between the reference satellite and the ground [from *Price and Sandwell,* 1998].

minimal surface deformation. Perpendicular baselines are inversely proportional to the "ambiguity height" [e.g., *Rosen et al.*, 1996], which is the elevation change required to alter the phase difference by one cycle (2π radians), and thus pairs with longer baselines are more sensitive to topography. For interferograms spanning the earthquake we chose pairs with the shortest possible perpendicular baselines to reduce topographic effects which may obscure surface deformation. Figure 4 shows the parallel and perpendicular baseline components of all the orbits we checked for this study, and Figure 5 shows our selected pairs with their respective perpendicular baselines.

2. To form interferograms, we used a SAR processor that employs a range-Doppler algorithm (see *Zebker et al.* [1994] and *Rosen et al.* [1996] for a broader and more specific description of the processing procedure). Generating an interferogram involves coregistration and matching of a group of images in a specific frame to subpixel resolution. Orbital locations of the satellite for each image were used to find the image that was roughly in the center of the group, and this image was designated as the master image, to which the others were matched. To match the images, we used an algorithm that is part of the Stanford/Jet Propulsion Laboratory interferometry processing package. This algorithm matches the amplitude of the images and outputs shift and stretch parameters, which are then input into the SAR processor. After the images have been matched, each complex pixel in a reference image is multiplied by the complex conjugate of the matching pixel in a repeat image. The result is a complex image whose phase components constitute the interferogram. The phases are ambiguous to within an integer number of 2π cycles ("wrapped", in INSAR terminology).

3. To form double-difference interferograms (topography-free), for each specific earthquake-spanning period we made two interferograms: one that spans the earthquake and the other that does not [*Zebker et al.*, 1998]. Because the total (unambiguous) phase of each point in the image is needed to obtain elevations for the topographic corrections, the phase of the nonearthquake interferogram was unwrapped by using the Residue-Cut Tree phase unwrapping algorithm proposed by *Goldstein et al.* [1988]. The unwrapped interferogram was then scaled to the earthquake interferogram by the ratio of their perpendicular baselines and subtracted from it. The resulting interferogram was then rewrapped to get the double-difference interferogram. The study area has rugged topography with long scarps where the slope exceeds 20°, and thus the phase could not be unwrapped across these boundaries. Fortunately, the region is extremely arid with little vegetation, resulting in high-correlation interferograms and facilitating the unwrapping. Moreover, many of the earthquake-spanning interferograms had very short baselines (<30 m), so unwrapping errors were not a major problem.

There is no standard method for removing orbital errors that produce artifacts, such as a false tilt across the

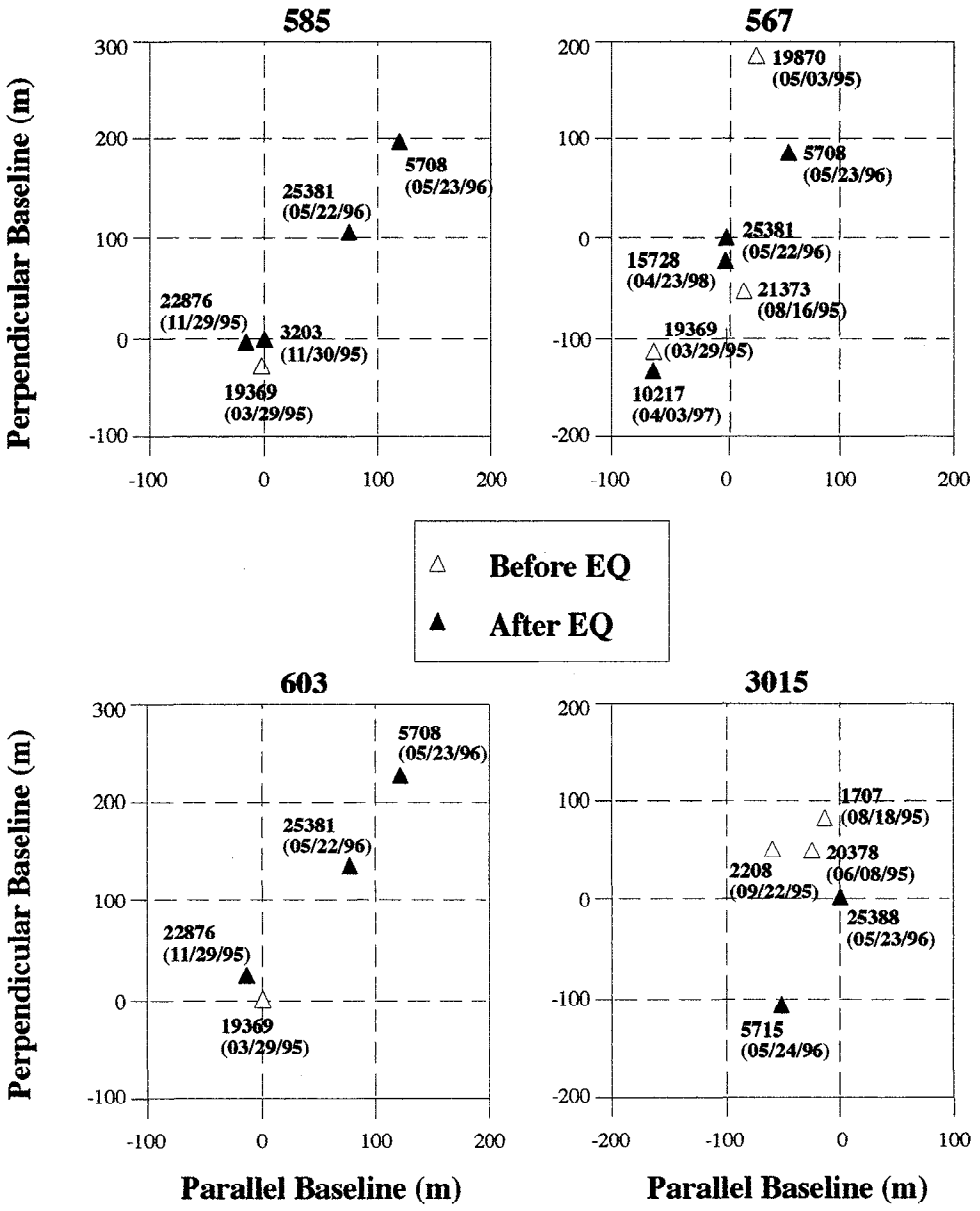

Figure 4. Parallel and perpendicular baselines of orbits checked for this study.

deformation interferogram. In previous studies [e.g., *Massonnet et al.*, 1993], orbital errors were corrected for by choosing an area in the interferogram where no deformation was assumed and subtracting the tilt of that area from the entire interferogram. A major drawback of this procedure is that in many cases the entire interferogram shows some deformation, and thus the subtracted signal also includes deformation. We approached this problem in two ways. First, we used precise orbital information provided by *Scharroo et al.* [1998]. Second, we used interferometric pairs that are of similar orbits as those analyzed for the earthquake but are from frame 603 (Figure 2), which is 150 km north of the earthquake and is not expected to show any deformation. The tilt of that interferogram was subtracted from the other double-difference interferograms to correct for orbital error; this procedure is plausible because, as seen below (Plate 2a), the orbital error is almost constant along the satellite track.

4. Coseismic Interferograms

Following the procedures described above, we generated coseismic interferograms for three frames that surround the earthquake rupture trace (567, 585, and 3015) and for frame 603, which is centered about 150 km north of the epicenter (Figure 2). Three distinct interferograms of frame 585 are shown in Plate 1: (1) an interferogram made from orbits 19369 and 22876 (Figure 4), 8 months before and 1 week after the earthquake, respectively, with a perpendicular baseline of 14 m (Plate 1a); (2) an interferogram made from a tandem pair of orbits 25381 (ERS-1) and 5708 (ERS-2) 6 months after the earthquake, with a perpendicular baseline of 93 m (Plate 1b); and (3) a double-difference (topography-free) interferogram generated by unwrapping, scaling, and subtracting the tandem interferogram from the earthquake interferogram (Plate 1c). The latter is the coseismic

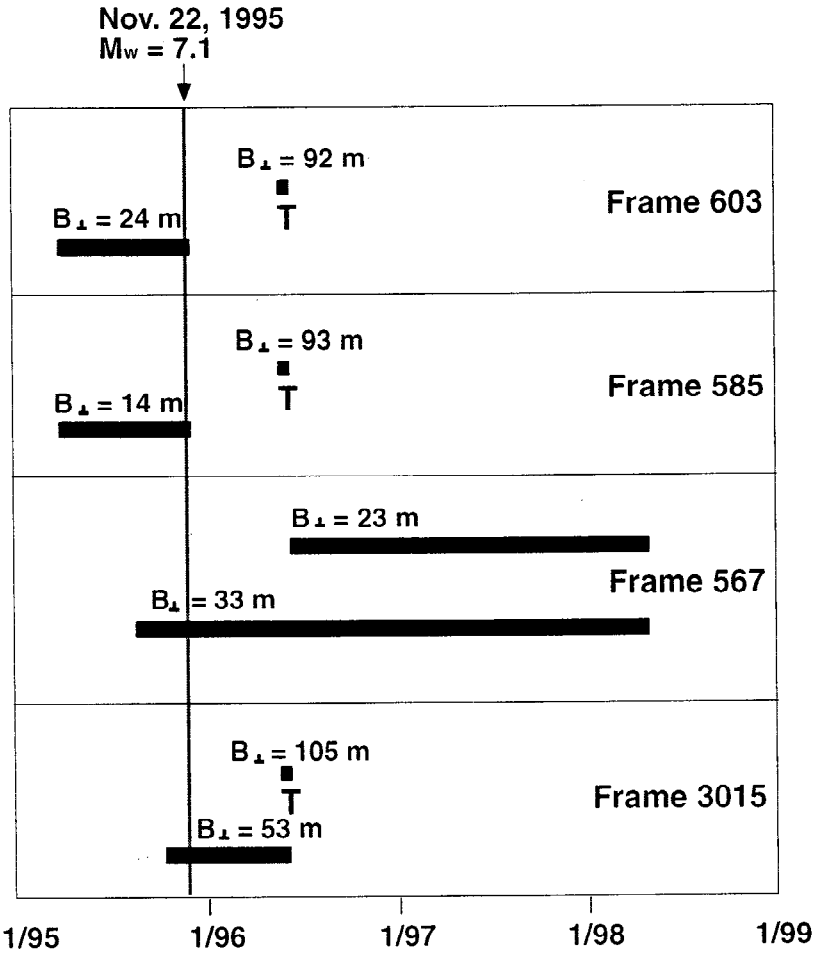

Figure 5. Selected interferometric pairs for this study, with their respective perpendicular baselines.

interferogram for frame 585. Some areas in this interferogram (and in other interferograms shown later) have very high topographic gradients; thus the phase due to topography in these areas could not be unwrapped and subtracted, and this phase remains in the topography-free interferogram. For example, the NE-SW trending band of irregular fringes in the top right side of Plate 1a is due to the steep eastern margin of the Arava Valley. These fringes cannot be unwrapped and are thus also seen in Plate 1c. They are even more dense and irregular in Plate 1b owing to the longer baseline of that pair.

Plate 2a combines the coseismic interferograms of all four frames. No orbital correction has been made yet. The three eastern frames seem to match fairly well, as fringes are continuous from one frame to the other. This observation, particularly the match of frames 585 and 567, is encouraging and somewhat surprising, because these two interferograms were generated from different orbits and span a different time interval (Plate 2a; see discussion below). An independent interferogram for frame 567, generated from different orbits (19369 and 10217), shows a strikingly similar fringe pattern as the interferogram shown in Plate 2a, which was made from orbits 21373 and 15728, lending additional support to the reliability of these results. The discontinuity between the eastern frames and frame 3015 is an inevitable consequence of the different viewing direction of the two tracks, which will become apparent in the model (synthetic) interferograms as well.

Frame 603 shows a tilt of 2-3 cycles across-track. This tilt continues southward into the NW corner of frame 585, but it is obscured in the central and southern parts of that frame by the deformation fringes. We believe that because frame 603 is centered about 150 km north of the epicenter, and the tilt does not resemble any of the deformation patterns in the southern part of frame 585, it was not formed by deformation and is most likely due to orbital errors. We therefore remove this tilt from frames 603 and 585 (which were created from the same orbits). The interferograms in frames 567 and 3015 were created from different orbits; thus we have no objective way to determine their orbital errors. However, since removing such a tilt from the interferogram of frame 567 preserves the fringe continuity between frames 585 and 567, we remove this tilt also from the interferograms of the other two frames to generate an orbit-corrected coseismic interferogram (Plate 2b). This correction is later justified by the comparison between the observed and synthetic interferograms.

The coseismic interferogram shows a clear difference between the deformation pattern on the two sides of the Gulf. A high displacement gradient (strain) is seen on the western side of the Gulf, 20-40 km south of Elat, whereas the displacement gradient is relatively moderate on the eastern side of the Gulf. To estimate the total satellite-to-ground range changes due to the earthquake, we count the fringes across the interferogram from north (where minimal displacement is assumed) to south and find that the total

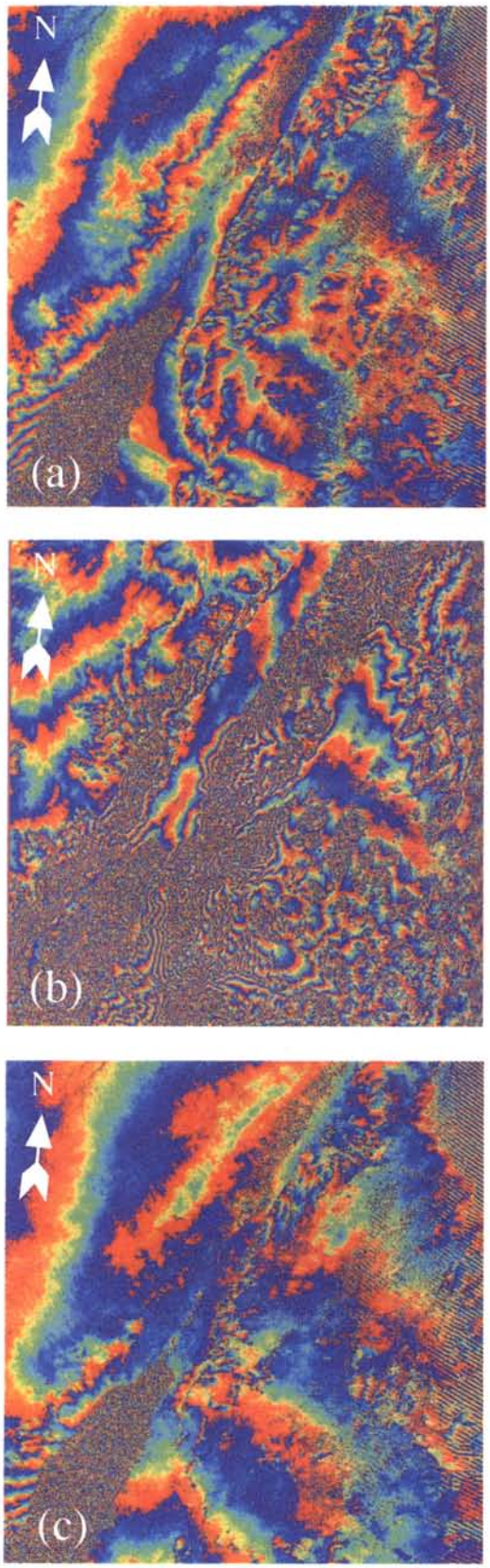

Plate 1. Interferograms of frame 585. (a) An interferogram made from orbits 19369 (March 23, 1995) and 22876 (November 29, 1995). Perpendicular baseline is 14 m. (b) An interferogram made from a tandem pair of orbits 25381 (May 22, 1996) and 5708 (May 23, 1996). Perpendicular baseline is 93 m. (c) A double-difference (topography-free) interferogram generated by unwrapping, scaling, and subtracting the tandem interferogram from the earthquake interferogram. The dimension of each interferogram is about 90 x 90 km.

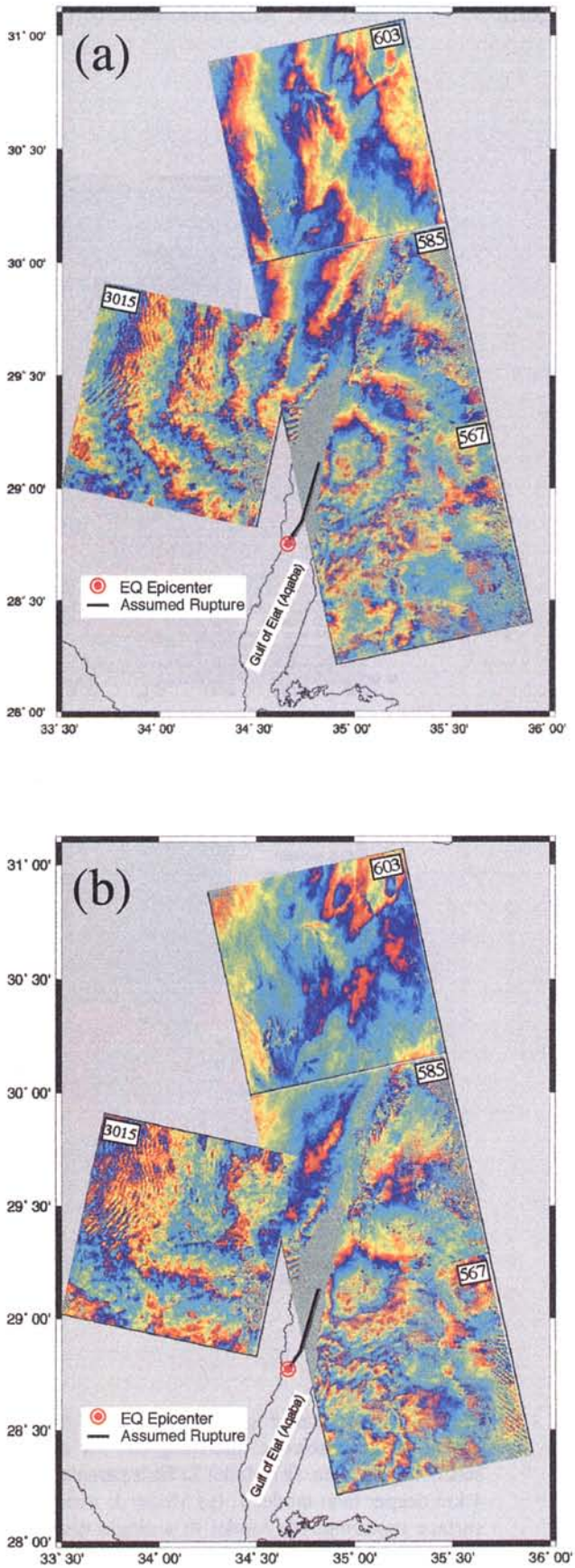

Plate 2. (a) Coseismic interferogram for all four frames, with no orbit correction. (b) Coseismic interferogram for all four frames, corrected for orbital errors. Note the short wavelength undulations in frame 3015, which are probably due to atmospheric effects.

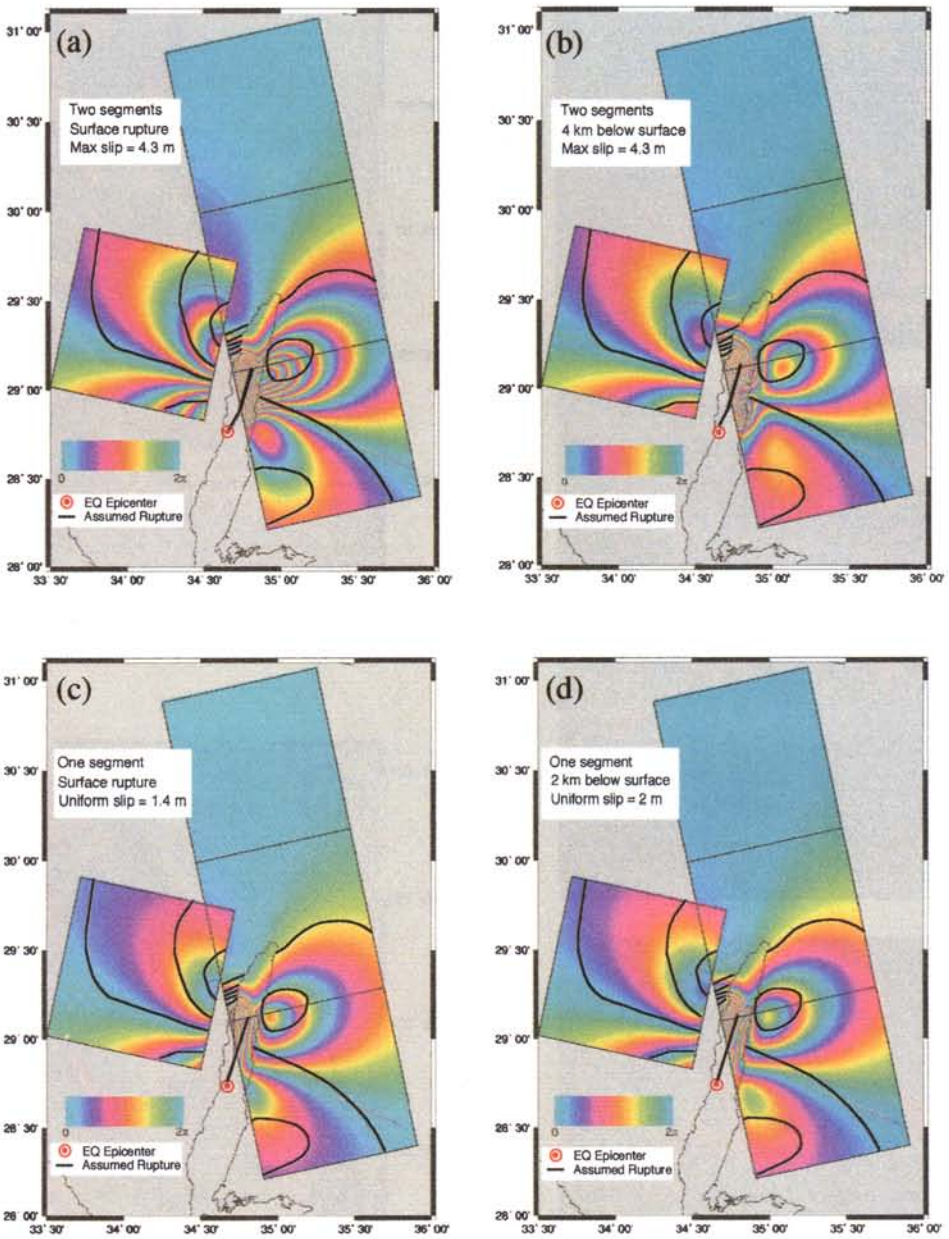

Plate 3. Model interferograms showing fringes calculated from a dislocation model. Solid lines represent 2π cycles of the coseismic interferogram, for comparison. (a) Model 1: fault parameters estimated from the seismological data. (b) Model 2: fault parameters estimated from the seismological data, but entire rupture is 4 km deeper than model 1. (c) Model 3: a single dislocation striking 017°, 45 km long, 1.4 m uniform slip, surface rupturing. (d) Model 4: a single dislocation striking 017°, 45 km long, 2 m uniform slip, top of dislocation 2 km below surface.

satellite-to-ground range changes are at least 15 cm (5 cycles) on the western side of the Gulf and 10 cm (3 cycles) on the eastern side of the Gulf. The postearthquake scenes of frames 585 and 603 were imaged 1 week after the earthquake, and those of frames 567 and 3015 were imaged 6 months after the earthquake. Thus the interferograms reflect the mainshock deformation superposed by the deformation in the following first week (585) or 6 months (567 and 3015) after the earthquake. The highest strain accumulation is observed west and northwest and east and southeast of the assumed northeastern rupture end (Plate 2). In the latter area we also find small-scale deformation features in the coseismic phase gradient maps (Figure 6), produced by subtracting the stacked phase gradient from the phase gradient spanning the earthquake (see *Price and Sandwell* [1998] for a more detailed description of the method). These features strike approximately N-S and are a few kilometers long and up to 1 km wide. It is difficult to determine their exact nature, but their association with the high strain seen in the interferograms and their appearance only in the earthquake spanning phase gradient maps support their seismic origin.

5. Coseismic Dislocation Modeling

Interferometric fringes represent projections of (three-dimensional) surface displacements onto (one-dimensional) range changes in the line of sight between the satellite and surface, possibly contaminated by systematic errors such as orbit and timing errors, atmospheric refraction, and topographic uncertainties. We modeled the coseismic fault rupture and the expected three-dimensional (3-D) surface displacement field by rectangular dislocations buried in an elastic half-space [*Okada*, 1985]. We start with the analysis of *Shamir* [1996], who used the seismologically derived static

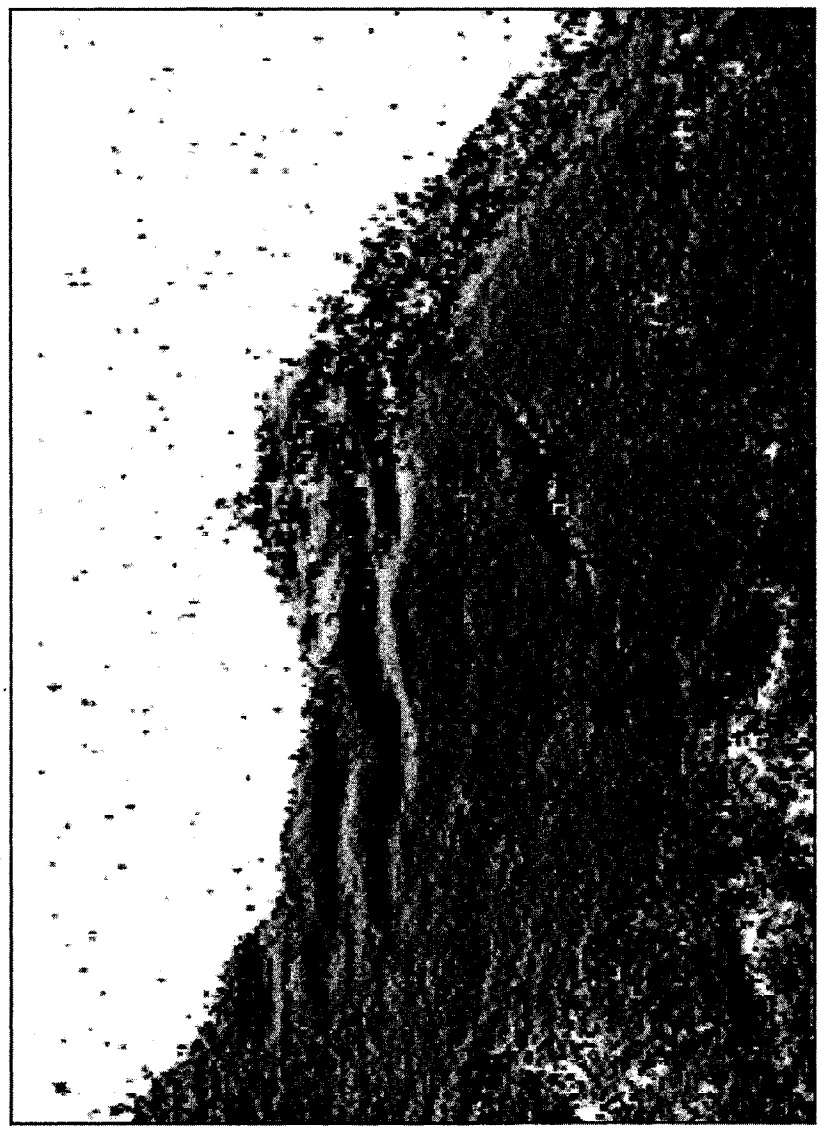

Figure 6. Interferogram deformation phase gradient map of coast-parallel lineaments along the eastern shore of the Gulf, 29.00°N, 34.88°E (see location in Figure 2), formed by subtracting scaled topographic phase gradient from coseismic phase gradient.

source parameters (epicenter, source dimension, source mechanism) estimated by *Kikuchi* [1995]. The rupture plane is described by 45 discrete segments, each of 1 km length. The model uses an overall elliptical slip distribution, as is commonly assumed for two-dimensional cracks in a homogeneous, linear-elastic medium loaded by uniform remote shear stress, with dislocations of 1.4 and 3.3 m for the first and second subevents, respectively. The average dislocation is assumed to be 3.2 m, with maximum slip of 4.3 m at the center of the second rupture. The down-dip slip is constant for each element, so the model is not fully 3-D. Then, by taking into account the satellite track direction and look angle, we formed a model (synthetic) interferogram by projecting the modeled 3-D displacements into the satellite-to-ground line of sight (see also *Feigl et al.* [1995]).

Comparison between the model (model 1, Plate 3a) and the coseismic interferograms shows agreement in the gross pattern but significant deviations in the details. The seismological model predicts a dense fringe pattern west of the assumed rupture termination, corresponding to the pattern found in the observed interferogram, implying that the length of the rupture and its strike are reasonable. This model also correctly predicts the different patterns on the two sides of the Gulf. However, the number of fringes (which correspond to the amount of surface displacement) is significantly higher in the model interferogram. We therefore maintain model rupture length and strike and adjust other fault parameters to obtain better agreement with the observed coseismic interferogram.

The smaller displacements implied by the coseismic interferogram suggest either that the amount of slip was smaller than in the seismological model, that the rupture was buried at depth, or both. To check these options, we first keep the slip values as in model 1 and incrementally increase the depth to the top of the rupture plane. The result (model 2, Plate 3b) shows that the greater the depth of the rupture plane, the smaller is the deformation at the medium range (10-50 km) east and west of the fault. The model interferograms become comparable to the coseismic interferogram only when the depth to the top of the rupture plane is about 4 km.

Next, we assume that surface rupturing did occur but that slip along the fault was smaller than suggested by *Shamir* [1996]. We generate a simplified model (model 3) consisting of only one dislocation, with length and average strike as in model 1, and with uniform slip. Model interferograms are produced for slip values between 1 and 3.5 m. The model interferogram deformation pattern shows a reasonable agreement with that of the coseismic interferogram for a mean slip value of about 1.4 m (Plate 3c). Thus, if surface rupture did occur, the observed interferograms indicate that the mean dislocation of the Nuweiba earthquake was about 1.4 m. Finally, we generate "intermediate" models that include both smaller slip and buried fault. Allowing 2 m slip on the fault (model 4), good agreement between the interferograms is found for 2 km depth (Plate 3d). It should be emphasized that good agreement is also found for a range of other combinations of slip and rupture depth.

6. Discussion and Conclusions

Since the Nuweiba earthquake rupture occurred within the central part of the Gulf of Elat, a strip of several kilometers on either side of the rupture was submarine, preventing us from observing any of the near-field deformation. Although significant deformation may cause phase decorrelation in a band that is up to 5 km wide on both sides of the fault [e.g., *Massonnet et al.*, 1993], the Gulf waters mask a wider belt, particularly east and southeast of the southern rupture termination and west and northwest of the northern termination. These regions may include some important near-fault fringe patterns that may constrain the slip distribution along the fault. However, the medium-range deformation patterns that are seen onshore are too far from the fault to be sensitive to the slip distribution, and therefore

Table 1. Comparison Between Seismological and INSAR Constraints on the Rupture Mechanism of the Nuweiba Earthquake

Parameter	Seismology	INSAR (This Study)
Rupture southern end, [a] deg	28.76N, 34.66E	28.76N, 34.66E
Rupture northern end, [a] deg	29.12N, 34.81E	29.15N, 34.80E
Rupture length, [a] km	~50	45-65
Rupture length, [b] km		45-65
I	20	
II	40	
Mechanism, [a] deg (strike, dip, rake)	203, 81, -7	197, 80, -14
Mechanism, [b] deg (strike, dip, rake)		
I	92, 38, -58	197, 80, -14
II	288, 82, -164	
Slip, [a] m	3.2	1.4-3
Slip, [b] m		
I	0.4	1.4-3
II	0.9	
Depth to top of rupture, [a] km	0 (surface rupturing)	0-4 km (slip dependent)

INSAR, interferometric synthetic aperture radar. I and II denote first and second subevents, respectively.

[a] *Shamir* [1996]

[b] *Pinar and Turkelli* [1997]

the coseismic interferograms of the Nuweiba earthquake do not set unique constraints on that parameter. On the other hand, the observable deformation is sensitive to the location of the rupture, its depth, and the average slip. There are several model solutions that are comparable to the coseismic interferogram (Plates 3b-d). Our analysis shows that they constrain the fault geometry quite well but cannot simultaneously constrain the slip and the depth of the fault patch.

While seismological observations provide constraints on the static source parameters, there are significant differences between the two published analyses of this earthquake [*Shamir*, 1996; *Pinar and Turkelli*, 1997] (Table 1). Our coseismic interferogram better agrees with the general deformation patterns derived from models that are based on *Shamir* [1996], particularly around the northern end of the rupture. If we adopt the seismologically derived mean dislocation of 3.2 m, then our results suggest that no surface rupturing occurred. On the other hand, if we assume that surface rupturing did occur (which is likely for an earthquake of that magnitude), then our results imply that other earthquake parameters (mean slip, rupture patch size) are different from the seismologically derived ones. Neither of our models, however, is fully three-dimensional, and it is likely that a dip-parallel slip gradient resulted in near-surface slip values which are much smaller than the average. This option combines surface rupturing with sufficiently low near-surface slip.

Of the four interferograms that are combined to produce the entire coseismic interferogram, two span the earthquake epoch by 1 week, and the other two span the earthquake epoch by 6 months. This implies that the deformation fringes are not necessarily only coseismic, but may also contain a postseismic component. However, despite the time difference, the 1 week and 6 month interferograms exhibit a similar deformation pattern, implying that whatever postseismic deformation occurred in the 6 months following the earthquake, most of it occurred during the first week. The fairly good agreement between the model results and this interferogram further indicates that postseismic deformation was either minor or confined to the near-fault region. A more detailed analysis of postseismic displacement for various time intervals following the earthquake should be carried out to provide a better estimate of the temporal and spatial extent of the postseismic transients. These effects are very important for understanding the way strain is accumulated and released along the DST and may have important implications for the occurrence of a future earthquake in this region.

Acknowledgments. This study was conducted with support from a grant to SIO jointly funded by NASA and NSF (NSF EAR-9619201). The SAR data used in this study was provided by the European Space Agency (ESA) and distributed by Eurimage Company. We wish to thank Abraham Tal for making the contacts, and Didier Massonnet for sharing with us some of his early SAR data. Evelyn Price and Karen Watson are thanked for their help in data processing. Ramon Hanssen and two anonymous reviewers are thanked for their critical and constructive reviews.

References

Alamri, A. M., Seismicity and aeromagnetic features of the Gulf of Aqaba (Elat) region, *J. Geophys. Res., 96*, 20,179-20,185, 1991.

Ambraseys, N. N., and C. P. Melville, Evidence for intraplate earthquakes in northwest Arabia, *Bull. Seismol. Soc. Am., 79*, 1279-1281, 1989.

Bartov, Y., G. Steinitz, M. Eyal, and Y. Eyal, Sinistral movements along the Gulf of Aqaba - Its age and relation to the opening of the Red Sea, *Nature, 285*, 220-221, 1980.

Bechor, N., Measurements of current tectonic movements in the Sinai Subplate using GPS observations, M.S. Thesis, 92 pp., Tel Aviv Univ., Tel Aviv, Israel, 1998.

Ben-Avraham, Z., Structural framework of the Gulf of Elat (Aqaba), *J. Geophys. Res., 90*, 703-726, 1985.

Ben-Avraham, Z., and G. Tibor, The northern edge of the Gulf of Elat, *Tectonophysics, 226*, 319-331, 1993.

Ben-Avraham, Z., G. Almagor, and Z. Garfunkel, Sediments and the structure of the Gulf of Elat (Aqaba), *Sediment. Geol., 23*, 239-267, 1979.

Bock, Y., and S. Williams, Integrated satellite interferometry in southern California, *Eos Trans. AGU, 78*(29), 293, 299-300, 1997.

Bock, Y., et al., Detection of crustal deformation from the Landers earthquake sequence using continuous geodetic measurements, *Nature, 361*, 337-340, 1993.

El Isa, Z. H., H. M. Marghelani, and M. A. Bazzari, The Gulf of Aqaba earthquake swarm of 1983 January-April, *Geophys. J. R. Astron. Soc., 78*, 711-722, 1984.

Eyal, M., Y. Eyal, Y. Bartov, and G. Steinitz, The tectonic development of the western margin of the Gulf of Elat (Aqaba) rift, *Tectonophysics, 80*, 39-66, 1981.

Eyal, Y., The tectonics of Shelomo and Yotam grabens, Elat, Israel, *Isr. J. Earth Sci., 22*, 165-184, 1973.

Feigl, K. L., A. Sergent, and D. Jacq, Estimation of an earthquake focal mechanism from a satellite radar interferogram: Application to the December 4, 1992 Landers aftershock, *Geophys. Res. Lett., 22*, 1037-1040, 1995.

Freund, R., The geometry of faulting in the Galilee, *Isr. J. Earth Sci., 19*, 117-140, 1970.

Goldstein, R. M., H. A. Zebker, and C. L. Werner, Satellite radar interferometry: Two-dimensional phase unwrapping, *Radio Sci., 23*, 713-720, 1988.

Hall, J. K., and Z. Ben-Avraham, Bathymetric chart of the Gulf of Elat, Geol. Surv. of Isr., Jerusalem, 1978.

Hofstetter, A., G. Shamir, and H. K. Thio, The 1995 Nuweiba source complexity and its relation with the aftershock sequence, paper presented at the 26th General Assembly of the European Seismological Commission, Tel Aviv, Israel, 1998.

Joffe, S., and Z. Garfunkel, Plate kinematics of the circum Red Sea - A re-evaluation, *Tectonophysics, 141*, 5-22, 1987.

Kikuchi, M., Teleseismic analysis of the Gulf of Aqaba, Egypt, earthquake of Nov. 22, 1995, *Seismol. Note 49*, 1995.

Kimata, F., A Tealeb, H. Murakami, N. Furukawa, S. Mahmoud, H. Khalil, K.O. Sakr, and A.M. Hamdy, The Aqaba Earthquake of November 22, 1995 and co-seismic deformation in Sinai Peninsula, deduced from repeated GPS measurements, *Acta Geod. Geoph. Hung., 32*(1-2), 53-71, 1997.

Massonnet, D., M. Rossi, C. Carmona, F. Adragna, G. Peltzer, K. Feigl, and T. Rabaue, The displacement field of the Landers earthquake mapped by radar interferometry, *Nature, 364*, 138-142, 1993.

Massonnet, D., K. L. Feigl, H. Vadon, and M. Rossi, Coseismic deformation field of the M = 6.7 Northridge, California earthquake of January 17, 1994 recorded by two radar satellites using interferometry, *Geophys. Res. Lett., 23*, 969-972, 1996.

Murakami, M., M. Tobita, S. Fujiwara, T. Saito, and H. Masaharu, Coseismic crustal deformation of 1994 Northridge, California, earthquake detected by interferometry, *J. Geophys. Res., 101*, 8605-8614, 1996.

Okada, Y., Surface deformation to shear and tensile faults in a half-space, *Bull. Seismol. Soc. Am., 75*, 1135-1154, 1985.

Ostrovsky, E., GPS data processing of EASTMED '95 campaign by commercial and scientific software packages, *Tech. Rep. TR-GSI/4/97*, 59 pp., Geol. Surv. of Isr., Jerusalem, 1997.

Ozawa, S., M. Murakami, S. Fujiwara, and M. Tobita, Synthetic aperture radar interferogram of the 1995 Kobe earthquake and its geodetic inversion, *Geophys. Res. Lett., 24*, 2327-2330, 1997.

Pinar, A., and N. Turkelli, Source inversion of the 1993 and 1995 Gulf of Aqaba earthquakes, *Tectonophysics, 283*, 279-288, 1997.

Price, E. J., and D. T. Sandwell, Small-scale deformations associated with the June 28, 1992, Landers, California, earthquake mapped by synthetic aperture radar interferometry phase gradients, *J. Geophys. Res., 103*, 27,001-27,016, 1998.

Quennel, A. M., Tectonics of the Dead Sea Rift, paper presented at the 20th International Geological Congress, Assoc. Serv. Geol. Africanos, Mexico 1956, 1959.

Rosen, P. A., S. Henseley, H. A. Zebker, F. H. Webb, and E. Fielding, Surface deformation and coherence measurements of Kilauea Volcano, Hawaii, from SIR-C radar interferometry, *J. Geophys. Res., 101*, 23,109-23,125, 1996.

Scharroo, R., P. A. N. M. Visser, and G. J. Mets, Precise orbit determination and gravity field improvement for the ERS satellites. *J. Geophys. Res., 103*, 8113-8127, 1998.

Segall, P., and J. L. Davis, GPS applications for geodynamics and earthquake studies, *Annu. Rev. Earth Planet. Sci., 25*, 301-336, 1997.

Shamir, G., The November 22, 1995, Nuweiba Earthquake, Gulf of Elat (Aqaba): Mechanical analysis, *Rep. 550/87/96 (114)*, Geophys. Inst. of Isr., Holon, 1996.

Shamir, G., and A. Shapira, Earthquake sequences in the Gulf of Elat, paper presented at the 27th General Assembly of the International Association of Seismology and Physics of the Earth's Interior, Wellington, New Zealand, 1994.

Tobita, M., et al., Deformation of the 1995 North Sakhalin earthquake detected by JERS-1/SAR interferometry, *Earth Planets Space, 50*, 313-325, 1998.

Wust, H., The November 22, 1995 Nuweiba earthquake, Gulf of Elat (Aqaba): Post-seismic analysis of failure features and seismic hazard implications, *Rep. GSI/3/97*, 58 pp., Geol. Surv. of Isr., Jerusalem, 1997.

Zebker, H.A., P.A. Rosen, R.M. Goldstein, A. Gabriel, and C.L. Werner, On the derivation of coseismic displacement fields using differential radar interferometry: The Landers earthquake, *J. Geophys. Res., 99*, 19,617-19,643, 1994.

G. Baer, Geological Survey of Israel, 30 Malkhe Yisrael Street, Jerusalem 95501, Israel. (baer@mail.gsi.gov.il)

Y. Bock, D. Sandwell, and S. Williams, Cecil H. and Ida M. Green Institute of Geophysics and Planetary Physics, Scripps Institution of Oceanography, La Jolla, CA 92093-0225 (ybock@igpp.ucsd.edu; sandwell@geosat.ucsd.edu; sdwil@mail.nerc-bidston.ac.uk)

G. Shamir, Geophysical Institute of Israel, P.O. Box 2286, Holon, Israel (gadi@iprg.energy.gov.il)

(Received January 5, 1999; revised May 11, 1999;
accepted June 16, 1999.)